3D Printing of Layered Vanadium Disulfide for Zinc-ion Batteries

Stefano Tagliaferri,[a] *Nagaraju Goli*[a], *Maria Sokolikova,*[a] *Rachael Quintin-Baxendale,*[a] *Cecilia Mattevi**[a]

[a] Department of Materials, Imperial College London, London SW7 2AZ, United Kingdom

*Corresponding author: c.mattevi@imperial.ac.uk

https://doi.org/10.26434/chemrxiv-2023-dh71k **ORCID:** https://orcid.org/0000-0002-7113-9398 Content not peer-reviewed by ChemRxiv. **License:** CC BY 4.0

Abstract

Aqueous zinc ion batteries are attractive energy storage devices for wearable electronics, owing to their safety and low cost. Among cathode materials, layered vanadium disulfide (VS_2) has demonstrated good charge storage capability, as a result of its metallic character and large interlayer spacing. However, VS_2 electrodes present fixed shapes and aspect ratios, and they are processed using toxic solvents, which hinders their integration in wearables. It is thus necessary to develop manufacturing methods that can meet the demand for shape customization and do not rely on toxic solvents. Here, we propose a flower-like VS_2 architectures using a simple hydrothermal process to formulate an ink for extrusion 3D Printing (Direct Ink Writing). The 3D printing technique enables the fabrication of VS_2 electrodes with porous micron-sized struts, high-mass loading of ~ 45 mg cm^{-2} and good conductivity. Using the 3D printed VS_2 cathodes, zinc-ion microbatteries were assembled, achieving a capacity of ~ 1.98 mAh cm^{-2} and demonstrating a capacity retention of over 55% after 150 cycles. The choice of the electrolyte and processing of the cathode ensured good stability against dissolution, a notorious challenge for VS_2 in aqueous environment. In particular, the dissolution of VS_2 cathodes for ZIBs was here prevented by the use of a water-in-salt electrolyte (WISE), enabling a long cycling life with higher capacity. This works paves the way towards form-free manufacturing of aqueous batteries which can be extended to different nanomaterials.

Introduction

The market of wearable devices is rapidly growing, demanding advanced energy storage systems that are safe, light and customizable.[1] The leading energy sources today are lithium-ion batteries (LIBs), and amongst those, lithium polymer batteries are the most commonly found in wearable devices. LIBs of these type can operate at > 3 V and reach an energy density 100-250 Wh kg^{-1}, making them the preferred choice for energy-demanding devices, such as mobile phones and portable electronic devices. Although these batteries show several advantages, such as high energy density and lightweight design, they also come with flammability concerns and high cost.[2] Additionally, hazardous organic solvents, such as N-Methyl-2-pyrrolidone (NMP) and organic carbonates, are employed in the manufacturing process of LIBs to cast the active materials and to dissolve the electrolyte salts. The manufacturing of lithium-ion batteries is typically based on slot-die coating under inert atmosphere, which limits the sizes and geometries available for the electrodes.[2–4] The safety and flammability of LIBs, alongside the limited shape customizability, may hinder their application in next generation healthcare wearable devices.[5–7] Wearable sensors typically present a power consumption in the order of ~ 0.01-1 mW, and require a nominal voltage > 1.5 V to operate,[8] thus opening to the possibility of using alternative chemistries to lithium. Zinc ion batteries (ZIBs) can be based on aqueous electrolytes and they present a lower cradle-to-gate environmental impact than LIBs in terms of CO_2 emissions per kWh of energy stored.[9] Zinc is an earth abundant element presenting a high theoretical capacity (~ 820 mAh g^{-1}), with a possibly high energy density and a conveniently low redox potential (− 0.76 V vs SHE) when used as anode in ZIBs.[10] Thus ZIBs can be regarded as a possible future alternative to LIBs for wearable devices.[9] On the other hand, the divalent nature of zinc and high charge density of zinc ions can be detrimental for the intercalation kinetic and the structural

https://doi.org/10.26434/chemrxiv-2023-dh71k **ORCID:** https://orcid.org/0000-0002-7113-9398 Content not peer-reviewed by ChemRxiv. **License:** CC BY 4.0

stability of cathode materials.[11] As a consequence, there is a general demand to identify suitable cathodes for zinc-ion batteries. Several polymorphs of MnO_2 (*e.g.* α-MnO_2, γ-MnO_2 and δ-MnO_2) have been investigated as high-performance ZIB cathodes, owing to their low cost and high theoretical capacity.[12] However, MnO_2 cathodes are often hindered by their low rate capability and cycling stability, associated with irreversible phase transitions and large volume change during cycling.[12,13]

Vanadium disulfide (VS_2) has been proposed as a high-performing cathode for ZIBs, owing to its layered structure with wide spacing between the layers (~ 5.76 Å), which can easily accommodate multivalent cations.[14] The high-valence vanadium centres in VS_2 promote redox reactions with fast kinetics. In contrast to other layered cathode materials (e.g. δ-MnO_2, with a conductivity lower than 10^{-5} S cm^{-1}),[15] the thermodynamically stable phase of VS_2 has metallic character, which is beneficial for electron transfer and rate performance. These favourable properties are reflected in the high capacity (205.3 mAh g^{-1}) and rate capability (135.4 mAh g^{-1} at 10 A g^{-1}) achieved when VS_2 is used as cathode for zinc-ion batteries, as demonstrated by Sun et al.[16] Additionally, Yu et al.[17] have recently shown that it is possible to induce the growth of a stable oxide layer on VS_2 cathodes by controlling the working potential of the zinc battery. The resulting VS_2/VO_x cathodes display higher capacity (301 mAh g^{-1}) and greater stability (75% capacity retention after 3000 at 1 A g^{-1}). However, VS_2-based cathodes raise some concerns in terms of structural dissolution and possible oxidation in aqueous $ZnSO_4$ electrolytes, which could affect the energy storage capability and long-term cycling. Several approaches have been proposed to mitigate the dissolution of vanadium-based electrodes in ZIBs, such as surface coatings, shape engineering, heterostructure formation and electrolyte optimization.[13,18] Particularly, adjusting the electrolyte concentration is an effective approach to mitigate the dissolution of VS_2 cathodes and regulate the extended cycling of ZIBs. In order to improve the energy storage performance, $ZnCl_2$ water-in-salt electrolytes (WISE) have been recently developed, presenting high concentrations (up to 31 mol per kg of solvent) than conventional $ZnSO_4$ electrolytes, which improves the performance and stability of the electroactive materials in the electrodes.[19,20] Meanwhile, VS_2 cathodes for ZIBs have been mainly investigated as coin and Swagelok cells, which are not fully compatible with lightweight wearable devices. Advanced manufacturing methods, able to meet the demand for batteries with customized shape, are yet to be demonstrated. 3D Printing is a versatile manufacturing technique that has drawn interest for the fabrication of form-free and miniaturized electrodes for energy storage devices. It enables the customization of the battery shape, which is a viable route to meet the requirements of wearable electronics. Additionally, it improves the electrochemical performance, owing to the higher areal loading of active materials and faster charge transport. On the other hand, the majority of studies on 3D Printed electrodes rely on NMP to disperse the active materials for ZIBs and obtain printable inks.[21–23] However, NMP presents toxicity concerns and its use aggravates the environmental impact of ZIBs, reducing the advantages over lithium-ion batteries.[24]

In this work, we demonstrate the use of extrusion-based 3D Printing (Direct Ink Writing) as a flexible manufacturing technique to fabricate VS_2 cathodes for aqueous zinc-ion batteries. The scalable hydrothermal synthesis employed for VS_2 ensures control over the morphology of the material, which can therefore be tailored for the 3D Printing process. We developed a novel ink formulation based on VS_2 for Direct Ink Writing and

https://doi.org/10.26434/chemrxiv-2023-dh71k **ORCID:** https://orcid.org/0000-0002-7113-9398 Content not peer-reviewed by ChemRxiv. **License:** CC BY 4.0

validated its printability through extensive rheological analysis. Importantly, the ink formulation here reported does not contain NMP and can be potentially applied to other cathode materials beyond VS_2. The cathode dissolution was effectively overcome using high-concentration water-in-salt electrolyte. The printed electrodes show a capacity of ~ 1.98 mAh cm^{-2} (~ 72 mAh g^{-1}) cycles in 30 m $ZnCl_2$, owing to a combination of diffusion-limited and pseudocapacitive charge storage processes. These results indicate the viability of 3D Printing to produce customizable energy storage devices, demonstrating the formulation of aqueous functional inks which can be produced at scale and printed in air, and a zinc-ion battery based on a new cathode material with a ~55% cycle stability up to 150 cycles.

Results and Discussion

Vanadium disulfide was synthesized *via* a simple hydrothermal method, using a small fraction of ethylene glycol as a co-solvent. A dimethyl sulfoxide (DMSO)-based ink was subsequently formulated from the hydrothermal VS_2, and employed to fabricate 3D printed cathodes, as illustrated in Scheme 1. The presence of ethylene glycol in the reaction system, with lower dielectric constant and higher viscosity than water, hinders the crystal growth and leads to the formation of small VS_2 microflowers ~ 5 μm in diameter (Figure 1-a,b).[25] Additionally, ethylene glycol can act as a reducing agent, helping to prevent the re-oxidation of V^{+4} to V^{+5} during the synthesis. In contrast, large VS_2 crystals and by-products are formed if ethylene glycol is not added (Figure S2). The microflower morphology is well suited for the extrusion-based 3D Printing process, since microflowers can be easily ejected throughout small nozzles (< 500 μm) without causing obstructions resulting in flow instabilities. The phase purity of hydrothermal VS_2 was demonstrated by EDS, XRD and Raman spectroscopy (Figure 1-c,d and Figure S1-a). All the XRD reflections can be assigned to the 1T phase of VS_2 (space group $P\bar{3}m1$); similarly, the Raman modes are comparable with previous reports of hydrothermally grown VS_2.[14,26] Bright field TEM imaging shows the atomically thin nature of the microflower petals (Figure 1-e), while HRTEM and SAED patterns (Figure 1-f,g) confirm that individual petals are made of highly crystalline areas, with the SAED pattern agreeing well with the (101) plane of 1T VS_2. This is consistent with previous studies on hydrothermal VS_2 displaying an unusually intense (101) reflection at 35.8º in the XRD pattern (Figure 1-c). The two doublets in the high-resolution XPS spectrum of V 2p (Figure 1-i) indicate the coexistence of two different oxidation states for vanadium on the surface of the microflowers, The doublet at higher binding energies (516.8 eV and 524.2 eV) agrees well with the values reported for the $2p_{3/2}$ and $2p_{1/2}$ core level electrons of V^{4+}.[27,28] The doublet at 513.7 eV and 521.4 eV corresponds to lower oxidation states, probably V^{3+}, originating from the reduction of the V^{5+} precursor during the synthesis or the possible presence of intercalated V atoms.[29] The S 2p spectrum (Figure 1-g) also present two doublets, indicating the presence of polysulfides (S_n^{2-}), which probably originate from the excess free sulfides in the reaction system.[30]

The VS_2 inks were formulated starting from a suspension of carbon black in DMSO. Carbon black particles are known to form loosely-interacting aggregates in suspension, that turn into a space-filling network of connected particles above a critical concentration.[31,32] Concentrated suspensions behave as elastic solids at rest, while being able to flow under the action of a sufficiently high stress (yield stress), which disrupts the

https://doi.org/10.26434/chemrxiv-2023-dh71k **ORCID:** https://orcid.org/0000-0002-7113-9398 Content not peer-reviewed by ChemRxiv. **License:** CC BY 4.0

connectivity of carbon black particles. The existence of a finite yield stress is a key property for extrusion-based printing, since each ink layer must retain its initial shape and support the weight of successive layers.[33] The critical concentration for carbon black suspensions in DMSO falls between 2.7 wt% and 5.3 wt%, as evidenced by oscillatory rheology (Figure 2-a,b). All the suspensions with concentration higher than 5.3 wt% present constant viscoelastic moduli in the range of frequency investigated (0.1 to 100 Hz), with a storage modulus significantly higher than the loss modulus, indicating a gel-like behaviour and a predominantly elastic response. On the contrary, the 2.7 wt% suspension exhibit a crossover point for the viscoelastic moduli at ~ 2 Hz, indicating a liquid (viscous) response in the limit of small frequencies (Figure S1-b).[34] The values of storage modulus and yield stress progressively increase with concentration, reaching ~30 kPa and ~235 Pa at 10 wt%, respectively. At higher concentrations the suspension becomes inhomogeneous and unsuitable for extrusion.

PVDF was added to the carbon black suspension as a binder, to retain the mechanical integrity of the printed structures after solvent evaporation. The as-obtained carbon black – PVDF paste can act as a conductive ink ($\sigma \sim 800$ S m^{-1}, Figure S1-c) for the printing of different energy storage materials. In specific, the addition of PVDF further increases the yield stress to ~400 Pa, as a result of the thickening effect of the polymer (Figure 2d). The final VS_2 ink was formulated by dispersing the hydrothermal microflowers into the carbon black – PVDF paste, achieving a yield stress ~450 Pa and storage modulus ~27 kPa (Figure S1-d and Figure 2-d). The VS_2 ink shows a shear thinning response during flow (Figure 2-e), which facilitates extrusion through fine printing nozzles. The shear thinning response can be attributed to the progressive disruption of the secondary interaction between carbon black and VS_2 particles under shear, resulting in suspended aggregates with smaller hydrodynamic volumes.[32] The reversibility of this process is fundamental to obtain self-standing structures that do not present buckling and lateral spreading on the substrate. In order to study the restructuring kinetic of the ink after shear, three interval thixotropy tests (3ITT) were performed on the final VS_2 ink (Figure 2-f). The ink was at first subjected to an oscillatory stress of 10 Pa (step 1 in Figure 2-f), which falls within the linear viscoelastic region of the ink and has no destructuring effect. After 120 s of equilibration, a high oscillatory stress of 450 Pa, approximately equal to the yield stress, was applied to the ink for 10 s to break the network structure (step 2 in Figure 2-f). Finally, an oscillatory stress of 10 Pa was applied again to the ink to study the microstructure rebuild (step 3 in Figure 2-f). After the high-stress step, the storage modulus instantly recovers to the equilibrium value, indicating the fast and reversible character of the destructuring process. Considering these favourable rheological properties, the VS_2 ink could be used to 3D print electrodes with woodpile geometry showing excellent shape retention after printing and drying (Figure 2-c and Figure S3).

The electrochemical properties of hydrothermal VS_2 cathodes were studied in a water-in-salt electrolyte (WISE) using zinc foil as the anode coated with a layer of carbon black. The role of the carbon coating was to inhibit the formation of dendrites, homogenizing the electric field and ion flux in the proximity of the anode, and retard the corrosion of zinc, which would cause capacity loss and decrease the cycling stability.[35–37] The highly concentrated electrolyte (30m $ZnCl_2$) was chosen to prevent the dissolution of VS_2 observed in conventional aqueous electrolytes. In contrast to previous works,[14,26] the dissolution of VS_2 in 3M $ZnSO_4$ was

https://doi.org/10.26434/chemrxiv-2023-dh71k **ORCID:** https://orcid.org/0000-0002-7113-9398 Content not peer-reviewed by ChemRxiv. **License:** CC BY 4.0

evidenced by a change in the colour of the solution, which turned bright yellow (Figure 3-a). The strong UV-vis absorption below ~ 550 nm can be attributed to the presence of VO_2^+ ions in the sample, resulting from the oxidation of VS_2 (Figure 2-b).[38] In contrast, the WISE electrolyte remained clear with no evident absorption peak in the visible range, which indicates the stability of VS_2 in the WISE electrolyte resulting from the absence of free uncoordinated water molecules.[39] Cyclic voltammograms in the conventional 3M $ZnSO_4$ electrolyte are characterized by a progressive reduction of the redox current caused by the dissolution of the active material (Figure S4-a), whereas the current progressively increases in the WISE electrolyte, until it reaches a stable value after 5 cycles (Figure S4-b). The WISE electrolyte also enables to access a larger potential window (1.5 V for 30m $ZnCl_2$ vs 1.2 V for 3M $ZnSO_4$) with no significant water decomposition. Plating-stripping tests on symmetric zinc foil cells indicate that the WISE electrolyte hampers the formation of dendrites and inert by-products, stabilizing the zinc anode for > 200 h at a high current density of 10 mA cm^{-2} (Figure S4-c). The cycling stability of symmetric cells were further extended with C@Zn electrodes, as presented in Figure S4-d. To better understand the nature of the redox processes in the cyclic voltammetry of VS_2, we conducted kinetic analysis by fitting the redox current with a power law:[40,41]

$$i = a\,\nu^b$$

where i is the redox peak current and ν the scan rate. When the value of b is ~ 0.5 the charge storage process is diffusion limited, while when $b \sim 1$ the charge storage has a capacitive nature. The first two oxidation peaks and the two corresponding reduction peaks (peaks 1,2,4 and 5 in Figure 3-c) have b values close to 0.5 (Table S1 and Figure 3-e,f), and they can be associated with the intercalation of Zn^{2+} ions into the layered structure of VS_2, similarly to a previous report.[14] Differently, the redox peaks at higher potentials (peaks 3 and 6 in Figure 3-c) have broader shape and the b values is closer to 1 (0.73 and 0.74 respectively). The latter suggests the presence of pseudocapacitive processes, likely to be associated with the surface oxidation of the VS_2 cathode.[17] As evidenced by ex-situ XRD (Figure 3d), there is no significant variation in the VS_2 peaks when the material is charged to different potentials, which support the evidence of the cathode stability during the first charging cycle. The shift in the (001) peak associated with zinc intercalation and reported in previous literature[14] cannot be resolved using ex-situ techniques, probably owing to the relaxation of the material during sample preparation.[42] Interestingly, a peak at ~ 23º appears at higher charge states, and it could be attributed to the (222) reflection of elemental sulfur, which can plausibly originate from the generation of sulfur vacancies in the material.[29] From XPS analysis during charge (Figure S8), the predominant oxidation state of V remains 4+, although a V^{5+} component also appears as a result of the surface oxidation process. During discharge, a doublet associated with V^{3+} appears, which can be related to the creation of sulfur vacancies.

The performance of 3D printed VS_2 was subsequently analysed and compared to tape-casted electrodes (Figure S5-a). The 3D printed VS_2 electrodes show significantly higher areal capacity (~ 4.98 mAh cm^{-2} vs ~ 0.48 mAh cm^{-2} after 10 cycles) as a consequence of the higher loading of VS_2 (Figure S5-a,b). Interestingly, the capacity of the printed cathode rapidly increases during the first ~ 10 cycles, before reaching a stable performance. The increase of capacity during this activation process can be attributed to the transformation of VS_2 into electrochemically-oxidised VS_2, as reported by Yang et al.[43] In order to prevent the electrochemical

https://doi.org/10.26434/chemrxiv-2023-dh71k **ORCID:** https://orcid.org/0000-0002-7113-9398 Content not peer-reviewed by ChemRxiv. **License:** CC BY 4.0

conversion of the material during operation, VS_2 electrodes were preliminary soaked in the WISE electrolyte for 14 days to promote the controlled growth of an electrochemically-active surface layer of oxide. SEM imaging demonstrates that the morphology of the microflowers is not altered during the conversion process (Figure S6-a). After 14 days of soaking, EDS and XRD evidence the presence of vanadium disulfide, indicating that only the surface layer of the microflowers is converted to amorphous oxide (Figure S6-b,c). The 3D printed VS_2 electrodes achieved an areal capacity of ~1.98 mAh cm^{-2} after soaking (*vs.* ~ 0.57 mAh cm^{-2} for bare 3D printed VS_2 electrodes in the first cycle, Figure S5), with a stable response even in the first charge-discharge cycles (Figure 4-c,f). In terms of gravimetric performance, 3D printed VS_2 electrodes achieved a stable gravimetric capacity of ~72 mAh g^{-1} at a current density of 36 mA g^{-1} (Figure S7). Owing to the high conductivity of the printed structures, the electrodes retained a capacity of ~ 0.88 mAh cm^{-2} when discharge at a high specific current of 7 mA cm^{-2} (Figure 4-d,e). Additionally, the soaking treatment ensured a high cycling stability, with a capacity retention higher than 55% after 150 cycles. The application of the 3D printed battery for portable electronics was demonstrated by encapsulating the electrodes inside a 3D printed case and using it to power an LED display (Figure 4-b).

Conclusions

In conclusions, we have here demonstrated the use of extrusion 3D Printing (Direct Ink Writing) to fabricate VS_2 electrodes for aqueous zinc ion batteries which are stable and cycle-life competitive with the current state of the art of VS_2 ZIBs. The VS_2 ink was optimized with suitable carbon loading to achieve high storage modulus at rest (~ 27 kPa), high yield stress (~ 450 Pa) and fast structural recovery after shear, demonstrating good printability. The VS_2 ink could thus be employed to fabricate 3D electrodes for aqueous ZIBs with a water-in-salt electrolyte (WISE). The WISE electrolyte in the zinc-ion battery effectively stabilized VS_2 against dissolution and enabled improved longevity. Specifically, the 3D printed battery electrodes supplied a capacity of ~ 1.98 mAh cm^{-2} and displays good reversibility up to 150 cycles with relatively stable charge and discharge curves. Benefiting from such stability, the ZIB could stably power an LCD display for several hours before discharge. These results demonstrate the feasibility of extrusion 3D Printing as an advanced manufacturing method for stable and miniaturized free-form zinc ion aqueous batteries based on arbitrary inorganic nanomaterials for portable and wearable electronic devices.

Materials and Methods

Hydrothermal synthesis of VS_2: VS_2 was synthesized by dissolving 11.2 mmol of Na_3VO_4 (Sigma-Aldrich) and 55.9 mmol of thioacetamide (Sigma-Aldrich) in 100 mL of deionized water and 40 mL of ethylene glycol. The solution was then transferred to a 200 mL PTFE-lined stainless-steel reactor and heated to 160°C for 24h. The reactor was naturally cooled to room temperature and the precipitate was washed three times with ethanol and dried in a vacuum oven for 2h at 70°C.

https://doi.org/10.26434/chemrxiv-2023-dh71k **ORCID:** https://orcid.org/0000-0002-7113-9398 Content not peer-reviewed by ChemRxiv. **License:** CC BY 4.0

Physical characterization: Scanning electron microscopy (SEM) images and EDS maps of the VS_2 microflowers were collected on a Zeiss Auriga SEM operated at an accelerating voltage of 5 kV (working distance ~ 5 mm). Powder X-ray diffraction was performed on the hydrothermal VS_2 with a Bruker D2 Phaser diffractometer equipped with a copper source in the range 2–60° for 2θ and with an angular step size of 0.034°. Raman spectra were acquired using a Renishaw inVia Qontor confocal Raman microscope at a wavelength of 532 nm. X-Ray photoelectron spectroscopy. XPS was performed using a Thermo Scientific K-Alpha+ with a monochromated Al X-ray source (hv = 1486.6 eV). The spectra were collected using pass energies of 200 eV for the survey and 20 eV for the core levels under a 200 μm spot size. HR TEM images and ADF STEM images were acquired on a JEOL JEM-2100F microscope with a field-emission gun operated at 200 kV accelerating voltage.

Ink formulation and 3D Printing: VS_2 inks were formulated by dispersing carbon black (acetylene, 100% compressed, Alfa Aesar) in dimethyl sulfoxide (DMSO) at 10wt% using a planetary mixer (Thinky ARE-250) at 1800 rpm for 2 min. Polyvinylidene fluoride (PVDF) was subsequently added to the mixture (PVDF:carbon black 1:1 weight ratio) and the resulting slurry was homogenized further 2 min at 1800 rpm. Finally hydrothermal VS_2 was ground in an agate mortar and added the slurry, which was again homogenized for 2 min at 1800 rpm. The final composition of the ink was 6:2:2 (VS_2:PVDF:carbon black) by mass. The conductivity of the carbon black slurries was measured with 4-probe tests using a Gamry Interface 1000 galvanostat. The rheological properties of the VS_2 ink were measured on a rotational rheometer (Discovery Hybrid Rheometer HR1 – TA Instruments) equipped with stainless-steel parallel plates (40 mm in diameter). Oscillatory stress sweeps were performed at a fixed frequency of 1 Hz, while oscillatory recovery tests were performed at 10 Hz to maximize the acquisition of points over time. Oscillatory frequency sweeps were conducted at a fixed strain amplitude of 0.1%, within the linear viscoelastic region of the VS_2 inks, as determined from the oscillatory stress sweeps. The inks were printed using an extrusion 3D printer with displacement-controlled plungers, at a feed rate of 6 mm s^{-1} and through 410 μm nozzles. After printing the electrodes were dried overnight at room temperature.

Cell assembly and electrochemical testing: Pouch-type cells were assembled using 30m $ZnCl_2$ electrolyte with glass fiber separators (Whatman GF/A with a thickness of 260 μm, Sigma-Aldrich). For zinc-ion batteries, zinc foil anodes (coated with a PVDF-carbon black protective layer) and 3D Printed VS_2 cathodes were used. For kinetic analysis a tape-casted electrode was used instead of a 3D printed one (slurry composition 7:2:1 VS2:carbon black:PVDF). Cyclic voltammetry (CV) and galvanostatic charge–discharge (GCD) and EIS curves were acquired using a multichannel VMP-3 workstation (Bio-Logic Science Instruments). The PLA cases for the zinc ion battery were fabricated *via* Fused Deposition Modelling (FDM), using a commercial Ultimaker 2+ printer.

https://doi.org/10.26434/chemrxiv-2023-dh71k **ORCID:** https://orcid.org/0000-0002-7113-9398 Content not peer-reviewed by ChemRxiv. **License:** CC BY 4.0

Acknowledgements

C. M. would like to acknowledge the award of funding from the European Research Council (ERC) under the European Union's Horizon 2020 research and innovation programme (Grant Agreement No. 819069), the award of a Royal Society University Research Fellowship (UF160539), by the UK Royal Society UK.

References

1. Liang, Y. *et al.* A review of rechargeable batteries for portable electronic devices. *InfoMat* **1**, 6–32 (2019).
2. Reddy, T. *Linden's Handbook of Batteries, 4th Edition*. (McGraw-Hill Education, 2010).
3. Gulbinska, M. K. Lithium-ion Cell Materials in Practice BT - Lithium-ion Battery Materials and Engineering: Current Topics and Problems from the Manufacturing Perspective. in (ed. Gulbinska, M. K.) 1–29 (Springer London, 2014). doi:10.1007/978-1-4471-6548-4_1.
4. Scrosati, B. & Garche, J. Lithium batteries: Status, prospects and future. *Journal of Power Sources* vol. 195 Preprint at https://doi.org/10.1016/j.jpowsour.2009.11.048 (2010).
5. Wu, H., Zhuo, D., Kong, D. & Cui, Y. Improving battery safety by early detection of internal shorting with a bifunctional separator. *Nat Commun* **5**, 5193 (2014).
6. Fan, X. *et al.* Flexible and Wearable Power Sources for Next-Generation Wearable Electronics. *Batter Supercaps* **3**, 1262–1274 (2020).
7. Chao, D. *et al.* Roadmap for advanced aqueous batteries: From design of materials to applications. *Sci Adv* **6**, eaba4098 (2023).
8. Gljušćić, P., Zelenika, S., Blažević, D. & Kamenar, E. Kinetic energy harvesting for wearable medical sensors. *Sensors (Switzerland)* **19**, (2019).
9. Iturrondobeitia, M., Akizu-Gardoki, O., Amondarain, O., Minguez, R. & Lizundia, E. Environmental Impacts of Aqueous Zinc Ion Batteries Based on Life Cycle Assessment. *Adv Sustain Syst* **6**, 2100308 (2022).
10. Li, C., Xie, X., Liang, S. & Zhou, J. Issues and Future Perspective on Zinc Metal Anode for Rechargeable Aqueous Zinc-ion Batteries. *ENERGY & ENVIRONMENTAL MATERIALS* **3**, 146–159 (2020).
11. Song, M., Tan, H., Chao, D. & Fan, H. J. Recent Advances in Zn-Ion Batteries. *Advanced Functional Materials* vol. 28 Preprint at https://doi.org/10.1002/adfm.201802564 (2018).
12. Xu, Y. *et al.* Recent Advances on Challenges and Strategies of Manganese Dioxide Cathodes for Aqueous Zinc-Ion Batteries. *Energy and Environmental Materials* Preprint at https://doi.org/10.1002/eem2.12575 (2022).
13. Wan, F. & Niu, Z. Design Strategies for Vanadium-based Aqueous Zinc-Ion Batteries. *Angewandte Chemie - International Edition* vol. 58 Preprint at https://doi.org/10.1002/anie.201903941 (2019).
14. He, P. *et al.* Layered VS2 Nanosheet-Based Aqueous Zn Ion Battery Cathode. *Adv Energy Mater* **7**, (2017).
15. Yan, L. *et al.* Modulating the electronic structure and pseudocapacitance of δ-MnO 2 through transitional metal M (M = Fe, Co and Ni) doping. *Electrochim Acta* **306**, (2019).
16. Sun, H. *et al.* Rose-like VS2 Nanosheets Chemically Anchored on Carbon Nanotubes for Flexible Zinc-Ion Batteries with Enhanced Properties. *ACS Appl Mater Interfaces* **14**, 40247–40256 (2022).

https://doi.org/10.26434/chemrxiv-2023-dh71k **ORCID:** https://orcid.org/0000-0002-7113-9398 Content not peer-reviewed by ChemRxiv. **License:** CC BY 4.0

17. Yu, D. *et al.* Boosting Zn2+ and NH4+ Storage in Aqueous Media via In-Situ Electrochemical Induced VS2/VOx Heterostructures. *Adv Funct Mater* **31**, (2021).

18. Liu, H. *et al.* Van der Waals Interaction-Driven Self-Assembly of V2O5Nanoplates and MXene for High-Performing Zinc-Ion Batteries by Suppressing Vanadium Dissolution. *ACS Nano* **16**, (2022).

19. Zhang, C. *et al.* A ZnCl2 water-in-salt electrolyte for a reversible Zn metal anode. *Chemical Communications* **54**, (2018).

20. Liang, T., Hou, R., Dou, Q., Zhang, H. & Yan, X. The Applications of Water-in-Salt Electrolytes in Electrochemical Energy Storage Devices. *Advanced Functional Materials* vol. 31 Preprint at https://doi.org/10.1002/adfm.202006749 (2021).

21. Ma, H. *et al.* 3D printing of solid-state zinc-ion microbatteries with ultrahigh capacity and high reversibility for wearable integration design. *J Power Sources* **550**, 232152 (2022).

22. Ma, H. *et al.* Tailoring Pore Structures of 3D Printed Cellular High-Loading Cathodes for Advanced Rechargeable Zinc-Ion Batteries. *Small* **17**, (2021).

23. Ren, Y. *et al.* CNT@MnO2 composite ink toward a flexible 3D printed micro-zinc-ion battery. *Carbon Energy* **4**, (2022).

24. Zhang, Y. S. *et al.* A Review of Lithium-Ion Battery Electrode Drying: Mechanisms and Metrology. *Advanced Energy Materials* vol. 12 Preprint at https://doi.org/10.1002/aenm.202102233 (2022).

25. Patil, S. A. *et al.* Solvent modulated self-assembled VS2 layered microstructure for electrocatalytic water and urea decomposition. *Int J Energy Res* **46**, (2022).

26. Liu, J., Peng, W., Li, Y., Zhang, F. & Fan, X. A VS2@N-doped carbon hybrid with strong interfacial interaction for high-performance rechargeable aqueous Zn-ion batteries. *J Mater Chem C Mater* **9**, (2021).

27. Hossain, M. *et al.* Chemical Vapor Deposition of 2D Vanadium Disulfide and Diselenide and Raman Characterization of the Phase Transitions. *Adv Mater Interfaces* **5**, (2018).

28. Wang, L., Huang, K. W., Chen, J. & Zheng, J. Ultralong cycle stability of aqueous zinc-ion batteries with zinc vanadium oxide cathodes. *Sci Adv* **5**, (2019).

29. He, L. *et al.* Defect-Engineered VS2 Electrocatalysts for Lithium–Sulfur Batteries. *Nano Lett* **23**, 7411–7418 (2023).

30. Gharabaghi, M., Irannajad, M. & Azadmehr, A. R. Selective sulphide precipitation of heavy metals from acidic polymetallic aqueous solution by thioacetamide. in *Industrial and Engineering Chemistry Research* vol. 51 (2012).

31. Youssry, M. *et al.* Non-aqueous carbon black suspensions for lithium-based redox flow batteries: Rheology and simultaneous rheo-electrical behavior. *Physical Chemistry Chemical Physics* **15**, (2013).

32. Wang, Y. & Ewoldt, R. H. New insights on carbon black suspension rheology—Anisotropic thixotropy and antithixotropy. *J Rheol (N Y N Y)* **66**, 937–953 (2022).

33. Tagliaferri, S., Panagiotopoulos, A. & Mattevi, C. Direct ink writing of energy materials. *Mater Adv* **2**, 540–563 (2021).

34. Trappe, V. & Weitz, D. A. Scaling of the viscoelasticity of weakly attractive particles. *Phys Rev Lett* **85**, (2000).

35. Xie, C. *et al.* Issues and solutions toward zinc anode in aqueous zinc-ion batteries: A mini review. *Carbon Energy* vol. 2 Preprint at https://doi.org/10.1002/cey2.67 (2020).

https://doi.org/10.26434/chemrxiv-2023-dh71k **ORCID:** https://orcid.org/0000-0002-7113-9398 Content not peer-reviewed by ChemRxiv. **License:** CC BY 4.0

36. Zhou, J. *et al.* Ultrathin Surface Coating of Nitrogen-Doped Graphene Enables Stable Zinc Anodes for Aqueous Zinc-Ion Batteries. *Advanced Materials* **33**, (2021).

37. Zhu, M. *et al.* A Patternable and In Situ Formed Polymeric Zinc Blanket for a Reversible Zinc Anode in a Skin-Mountable Microbattery. *Advanced Materials* **33**, (2021).

38. Choi, N. H., Kwon, S. & Kim, H. Analysis of the Oxidation of the V(II) by Dissolved Oxygen Using UV-Visible Spectrophotometry in a Vanadium Redox Flow Battery. *J Electrochem Soc* **160**, (2013).

39. Chen, C. Y., Matsumoto, K., Kubota, K., Hagiwara, R. & Xu, Q. A Room-Temperature Molten Hydrate Electrolyte for Rechargeable Zinc–Air Batteries. *Adv Energy Mater* **9**, (2019).

40. Wan, F. *et al.* Aqueous rechargeable zinc/sodium vanadate batteries with enhanced performance from simultaneous insertion of dual carriers. *Nat Commun* **9**, (2018).

41. Brezesinski, T., Wang, J., Tolbert, S. H. & Dunn, B. Ordered mesoporous α-MoO3 with iso-oriented nanocrystalline walls for thin-film pseudocapacitors. *Nat Mater* **9**, (2010).

42. Shadike, Z. *et al.* Advanced Characterization Techniques for Sodium-Ion Battery Studies. *Advanced Energy Materials* vol. 8 Preprint at https://doi.org/10.1002/aenm.201702588 (2018).

43. Yang, M. *et al.* Boosting the zinc ion storage capacity and cycling stability of interlayer-expanded vanadium disulfide through in-situ electrochemical oxidation strategy. *J Colloid Interface Sci* **607**, 68–75 (2022).

https://doi.org/10.26434/chemrxiv-2023-dh71k **ORCID:** https://orcid.org/0000-0002-7113-9398 Content not peer-reviewed by ChemRxiv. **License:** CC BY 4.0

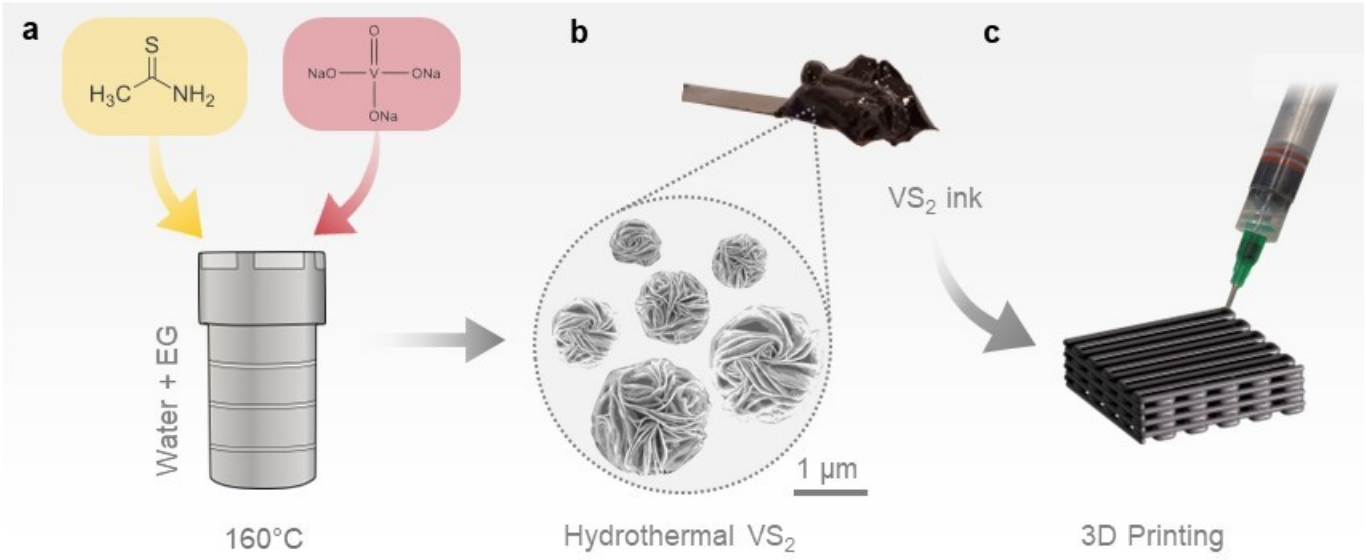

Scheme 1: Schematic showing the synthesis of the hydrothermal VS_2 microflowers (a), the formulation of VS_2 inks (b) and the 3D Printing of VS_2 inks to fabricate battery and supercapacitor electrodes (c)

https://doi.org/10.26434/chemrxiv-2023-dh71k **ORCID:** https://orcid.org/0000-0002-7113-9398 Content not peer-reviewed by ChemRxiv. **License:** CC BY 4.0

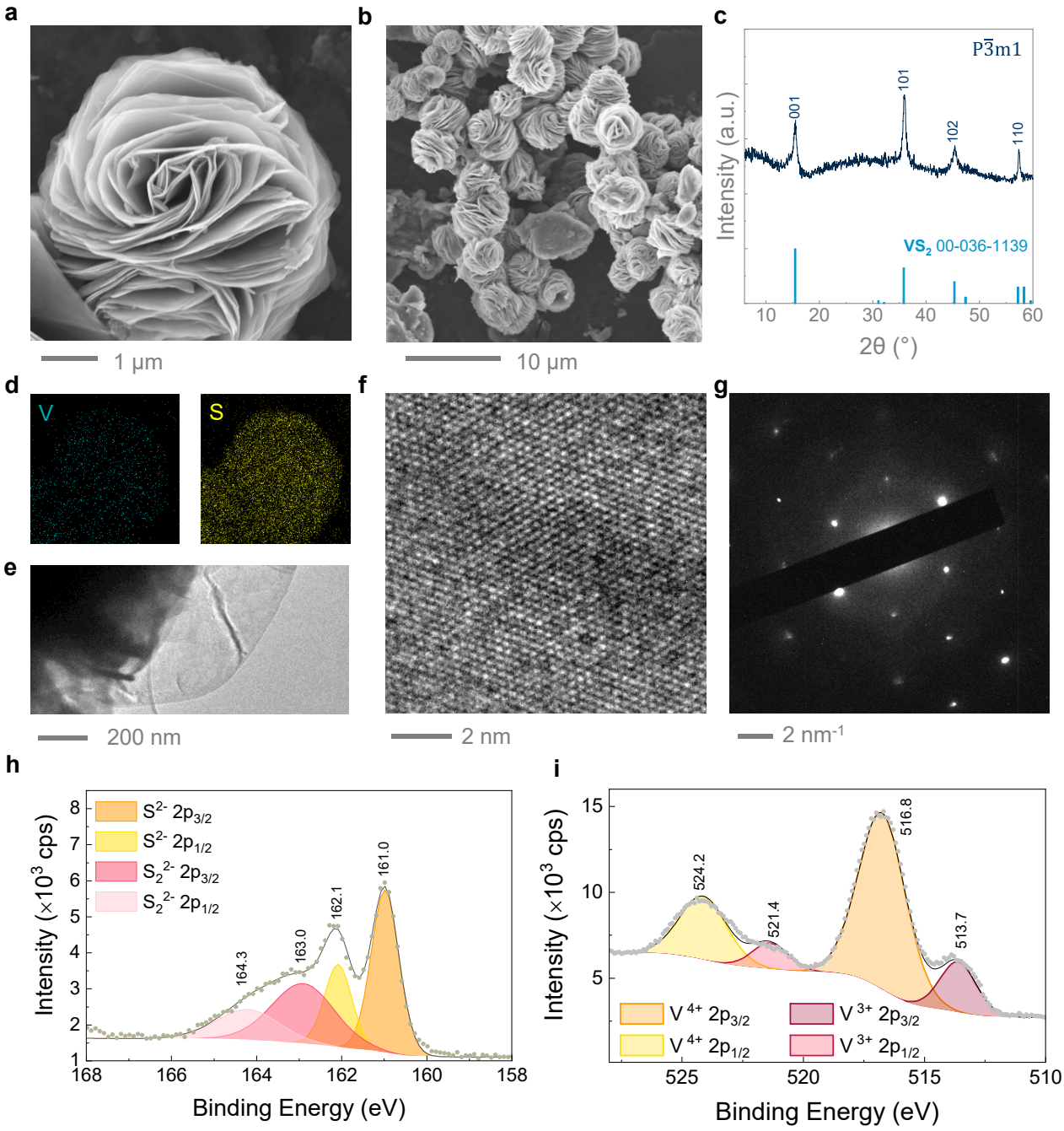

Figure 1: a,b) SEM images of VS_2 microflower; c) Powder XRD pattern for the hydrothermal VS_2 microflowers: d) EDS spectrum on the VS_2 microflower; e) TEM and f) HRTEM of a VS_2 petal; g) SAED pattern of hydrothermal VS_2 along the (101) plane, h,i) XPS analysis on the VS_2 microflowers, high-resolution spectra corresponding to S 2p (h) and V 2p (i).

https://doi.org/10.26434/chemrxiv-2023-dh71k **ORCID:** https://orcid.org/0000-0002-7113-9398 Content not peer-reviewed by ChemRxiv. **License:** CC BY 4.0

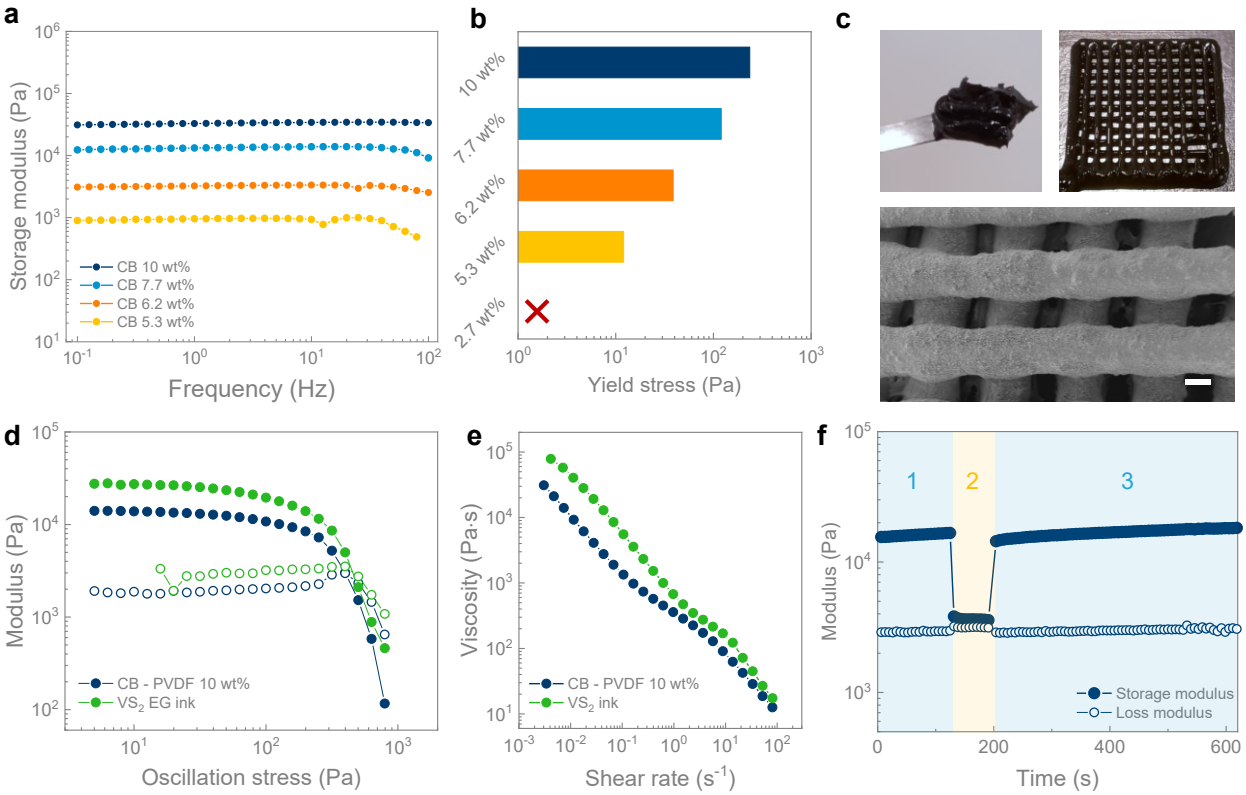

Figure 2: a) Oscillatory rheology (frequency sweep) of carbon black dispersions in DMSO at different concentrations; b) yield stress for different carbon black dispersions in DMSO; c) digital photographs and SEM images of the VS_2 ink (top left panel) and of a printed VS_2 electrode (woodpile structure in the top right and bottom panel, the scale bar is 200 µm); d) amplitude sweep for the carbon black-PVDF slurry and for the final VS_2 ink; e) flow ramp for the carbon black-PVDF slurry and for the final VS_2 ink; f) three interval thixotropy tests on the VS2 ink (step 1 and 3 at a shear stress of 10 Pa, step 2 at a shear stress of 450 Pa).

https://doi.org/10.26434/chemrxiv-2023-dh71k **ORCID:** https://orcid.org/0000-0002-7113-9398 Content not peer-reviewed by ChemRxiv. **License:** CC BY 4.0

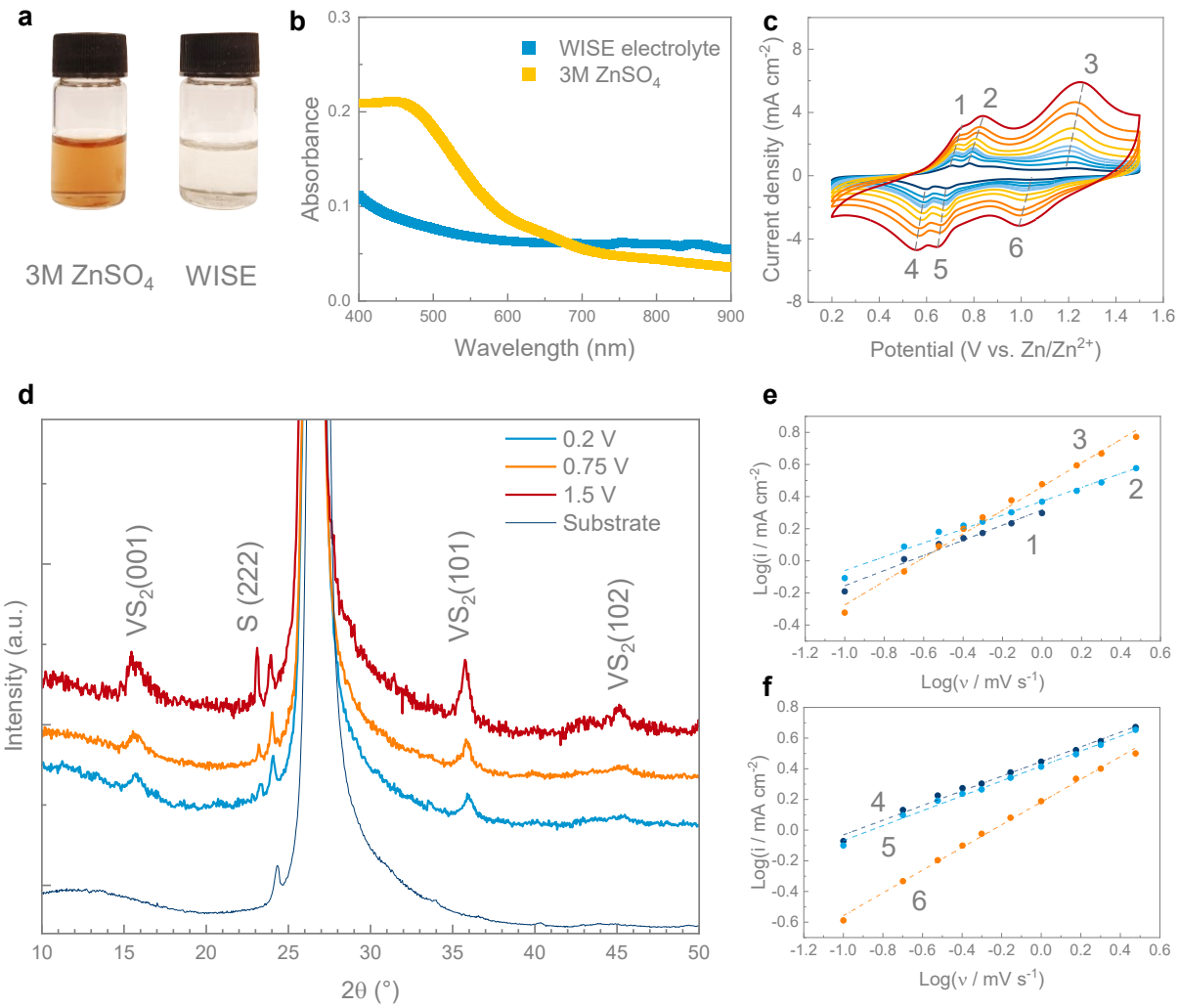

Figure 3: a) Digital photograph of the 3M $ZnSO_4$ and WISE electrolytes after ~ 100 h soaking of VS_2; b) UV-vis spectra of the 3M $ZnSO_4$ and WISE electrolytes after ~ 100 h soaking of VS_2; c) cyclic voltammetry on the tape-casted electrodes for kinetic analysis; d) *ex-situ* XRD on the VS_2 cathodes at different state of charge; e and f) power law fitting of the redox peak currents.

https://doi.org/10.26434/chemrxiv-2023-dh71k **ORCID:** https://orcid.org/0000-0002-7113-9398 Content not peer-reviewed by ChemRxiv. **License:** CC BY 4.0

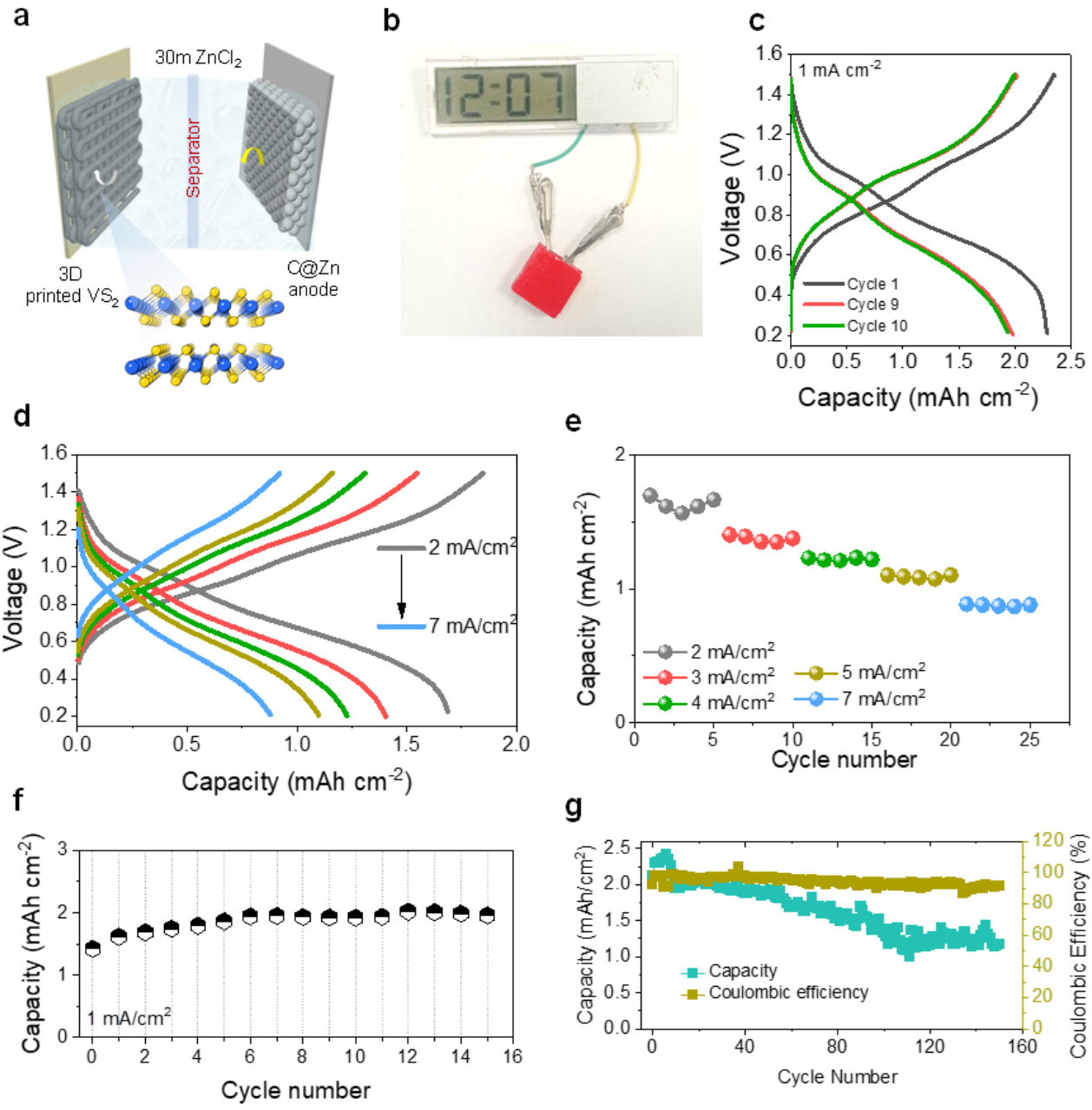

Figure 4: a) Schematic showing the zinc-ion battery with the 3D printed VS_2 cathode; b) encapsulated zinc ion battery powering a LCD display; c) charge-discharge curves at 1 mA cm^{-2} of the zinc-ion battery with a 3D printed VS_2 cathode; d,e) rate capability of the zinc-ion battery with a 3D printed VS_2 cathode; f,g) capacity during the first 15 cycles and capacity retention over prolonged cycling of the 3D printed VS_2 cathode.

https://doi.org/10.26434/chemrxiv-2023-dh71k **ORCID:** https://orcid.org/0000-0002-7113-9398 Content not peer-reviewed by ChemRxiv. **License:** CC BY 4.0